Electron. Mater. Lett., Vol. 13, No. 5 (2017), pp. 427-433
DOI: 10.1007/s13391-017-6258-7

Facile Synthesis of Hierarchical $CoMn_2O_4$ Microspheres with Porous and Micro-/Nanostructural Morphology as Anode Electrodes for Lithium-Ion Batteries

Yana Li[1,2], Xianhua Hou[1,2], Yajie Li[1,2], Qiang Ru[1,2], Shaofeng Wang[1,2], Shejun Hu[1,2], and Kwok-ho Lam[3,*]

[1]Guangdong Engineering Technology Research Center of Efficient Green Energy and Environmental Protection Materials, Guangzhou 510006, China
[2]Guangdong Provincial Key Laboratory of Quantum Engineering and Quantum Materials, School of Physics and Telecommunication Engineering, South China Normal University, Guangzhou 510006, China
[3]Department of Electrical Engineering, The Hong Kong Polytechnic University, Hunghom Kowloon 999077, Hong Kong

(received date: 7 August 2016 / accepted date: 17 October 2016 / published date: 10 September 2017)

Hierarchical $CoMn_2O_4$ microspheres assembled by nanoparticles have been successfully synthesized by a facile hydrothermal method and a subsequent annealing treatment. XRD detection indicate the crystal structure. SEM and TEM results reveal the 3-dimensional porous and micro-/nanostructural microsphere assembled by nanoparticles with a size of 20-100 nm. The $CoMn_2O_4$ electrode show initial specific discharge capacity of approximately 1546 mAh/g at the current rates 100 mA/g with a coulombic efficiency of 66.7% and remarkable specific capacities (1029-485 mAh/g) at various current rates (100-2800 mA/g).

Keywords: $CoMn_2O_4$ microspheres, hydrothermal method, crystal structure, lithium ion batteries

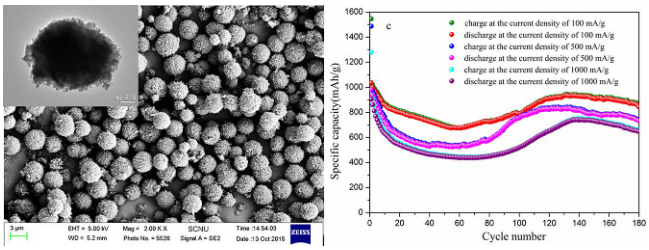

1. INTRODUCTION

Lithium-ion batteries (LIBs) are widely used as energy storage devices for not only popular portable devices but also up-coming electric vehicles.[1-3] Graphite has served as a reliable anode material for commercial LIBs, but it hardly meets the increasing demand due to low theoretical capacity (372 mAh/g).[4,5] The ever-growing demand for high capacity and/or high power LIBs has prompted tremendous research efforts in developing advanced high-performance electrode materials. Amongst the available materials, transition metal oxides (TMOs) materials have been widely studied and become one of the most promising anode materials for the next generation of lithium ion batteries (LIBs). Among various metal oxides, due to their many advantages, such as high theoretical capacity, low cost, abundant resources and environmental friendliness, low operating voltage and so on, ternary cobalt manganate ($CoMn_2O_4$) with spinel structure has been considered as a promising electrochemical candidate.[6,7] Myriad micro/nanostructures of Mn-based binary and ternary oxides, have been successfully synthesized and excellent lithium storage properties have been obtained. For example, Liu *et al.* compounded $CoMn_2O_4$ hierarchical twin-microspheres, it still retains discharge capacity of 573 mAh/g after more than 50 cycles at a high current density of 1000 mA/g, corresponding to 77% of the second-cycle discharge

*Corresponding author: houxh@scnu.edu.cn

capacity.[8] Lou *et al*. synthesized double-shelled $CoMn_2O_4$ hollow microcubes, which retained 624 mAh/g after 50 cycles and had a high capacity of 830 mAh/g at a current density of 200 mA/g.[9] Li *et al*. fabricated uniform hierarchical porous $CoMn_2O_4$ microspheres (3-6 μm) through a solvothermal process followed by a post-annealing treatment, the $CoMn_2O_4$ exhibit an initial capacity of 1107 mAh/g and the capacity is maintained at 420 mA h/g after 1000 cycles.[10]

However, the real performance of $CoMn_2O_4$ anodes, such as poor cycling stability, low rate capabilities, and high operating voltages still need further improvement to satisfy energy storage systems with high energy and power densities.[11,12] As established by related research, porous architectures assembled by numerous subclasses of nano-building blocks opened up accessible routes to enhance the reverse capacity and rate capability. We have been successfully synthesized the porous and micro-/nano-structural microsphere assembled by nanoparticles with a size of 20-100 nm by a facile solvothermal route and a subsequent annealing treatment. The initial specific discharge capacity is approximately 1546 mAh/g with a coulombic efficiency of 67.0% and the specific capacities is 1029-485 mAh/g at various current rates (100-2800 mA/g). The good cycling stability for highly reversible lithium storage of $CoMn_2O_4$ microspheres can be attributed to the unique assembled architecture and probably synergetic effects of different metal ions. Moreover, The porous construction served as free transportation channels for Li ions to move into the bulk of the electrode, shortening the whole diffusion duration. Furthermore, the assembled structure could well buffer the volume variation to maintain the good mechanical strength during repeated lithium ions insertion/extraction.[13] Besides, as we all know that materials composed of spherical particles have higher tap densities than those composed of irregular particles.[14,15]

2. EXPERIMENTAL PROCEDURE

2.1 Material synthesis

All chemicals (received from Sinopharm Chemical Reagent Co., Ltd.) used in the experiment were of analytic grade used without any further purification. In a typical synthesis, 1.66 g $Co(CH_3COO)_2 \cdot 4H_2O$, 3.27 g $Mn(CH_3COO)_2 \cdot 4H_2O$ were dissolved in 64 mL of ethylene glycol with constant stirring for 1 h. Then 4.20 g hexamethylenetetramine was introduced into the mixed solution and stirred for another 0.5 h till precipitate was disappeared. Subsequently, the homogeneous solution was transferred into a Teflon-lined stainless steel autoclave (100 mL in volume) and treated hydrothermally at 160 °C for 6 h to get the precipitate of $CoMn_2O_4$ particles. The resulting precipitate was then centrifuged, washed with distilled water and ethanol and then dried in an oven at 60 °C. Finally, the obtained $CoMn_2O_4$ particles were annealed at 300 °C for 2 h, and another 2 h at 500 °C in air atmosphere in the oven at a heating rate of 2 °C/min to form mesoporous $CoMn_2O_4$ microspheres.

2.2 Materials characterization and electrochemical measurement

The crystallographic phase of as-synthesized sample was characterized by powder X-ray diffraction (XRD, PANalytical X'Pert PRO, Cu_α radiation, $\lambda = 1.5406$ nm). The morphological investigation was carried out with scanning electron microscopy (SEM, ZEISS ULTRA 55). Structural and compositional information was provided by transmission electron microscope (TEM, JEM-2100HR) with Energy Dispersive Spectrometer (EDS), high-resolution TEM (HRTEM). The element contents were examined by energy-dispersive X-ray spectroscopy (EDS).

The active material ($CoMn_2O_4$ microspheres), conductive material (acetylene black), and polymer binder (polyvinylidene Fluoride, PVDF) were stirred for 3 h at a weight ratio of 80 : 10 : 10, and then coated on the surface of the copper foil. The working electrode had a diameter of 12 mm, with a coating thickness of 15 mm. The electrochemical measurements were carried out using coin-type half-cells (CR2530) assembled in an argon-filled glove box with both the moisture and the oxygen content below 1 ppm. 1 M $LiPF_6$ in a mixture of ethylene carbonate (EC), dimethylcarbonate (DMC) and diethyl carbonate (DEC) (1:1:1 by volume, provided by Cheil Industries Inc., South Korea) was used as the electrolyte. High purity Li (Aldrich) was used to prepare counter and reference electrode. The separator was made of a Celgard 2400 film. The galvanostatic charge-discharge data were collected by CT2001A LAND Cell test system at different current densities. The cyclic voltammetry (CV) was performed using electrochemical workstation (1470E, Solartron Analytical) at a scan rate of 0.1 mV/s in the range of 0.0-3.0 V. Impedance measurements were acquired in the frequency ranging from 0.01 Hz to 100 kHz. Results of the study are presented below.

3. RESULTS AND DISCUSSION

XRD patterns of the product synthesized before and after calcination are shown in Fig. 1. The diffraction peaks matched pretty well with those of body-centered-tetragonal $CoMn_2O_4$ (JCPDS card no. 77-0471, $a = b = 5.784$ Å, $c = 9.091$ Å, $\alpha = \beta = \gamma = 90$ °; space group: $I4_1/amd$) with a distorted spinel structure due to the well-known Jahn-Teller effect of manganese (III). No residues or contaminants have been detected, showing the high purity of the sample. The illustration in Fig. 1 demonstrates the schematic crystal structure of spinel $CoMn_2O_4$. In the spinel structure, the

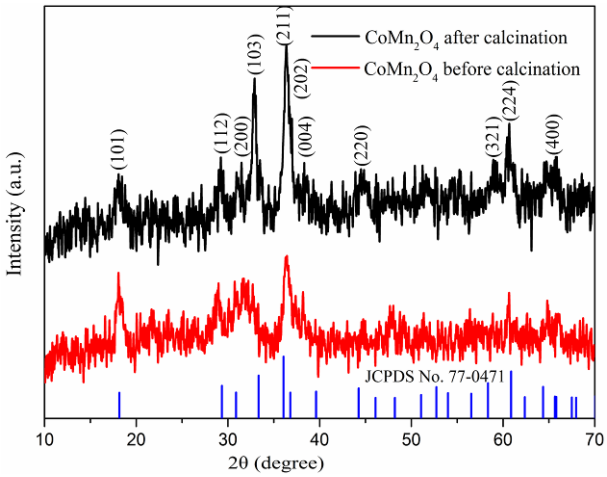

Fig. 1. XRD patterns of hierarchical $CoMn_2O_4$ microspheres before calcination and after calcination.

bivalent Co-ions and trivalent Mn-ions occupy the tetrahedral and octahedral void sites, which are isostructural to Co_3O_4.[16-18] In addition, the sharpening of the peaks is observed after the calcination process, indicating the improvement in crystalline quality.

Despite the high temperature post-treatment, the $CoMn_2O_4$ sample still retained the spherical morphology. Figure 2a, b depicts a low-magnification SEM image of the $CoMn_2O_4$ products with a diameters of about 600 nm. It can be seen that the product is composed of numerous uniform nanosized spherical particles. High-magnification FESEM examination (Fig. 2c, d) clearly indicated the detailed structural composition of the as-obtained microspheres. We can see that they are porous and composed of numerous closely packed primary nanoparticle in the size of 20-100 nm, whereby a large number of voids are left between adjacent nanoparticles. This appealing structural feature would greatly increase electroactive sites for efficient electrochemical energy storage, and favor the rapid mass transport meanwhile.[19,20] EDS spectrum of $CoMn_2O_4$ microspheres is illustrated in Fig. 2f. The lines of Mn, Co and O are obviously observed. In the inset of Fig. 2f, the chemical composition of the spinel $CoMn_2O_4$ is detected by energy-dispersive X-ray (EDX) spectroscopy analysis, which shows a Mn/Co ratio of 2. The dot mapping images shown in Fig. 2g, h, i showed Co, Mn and O components are uniformly distributed inside the $CoMn_2O_4$ mesoporous microspheres, in which a phase separation of Co and Mn components was not observed. implying that the as-prepared porous and micro-/nanostructural $CoMn_2O_4$ microspheres is a uniformly dispersed bicomponent nanocomposite.

A typical TEM image in Fig. 3a shows that $CoMn_2O_4$

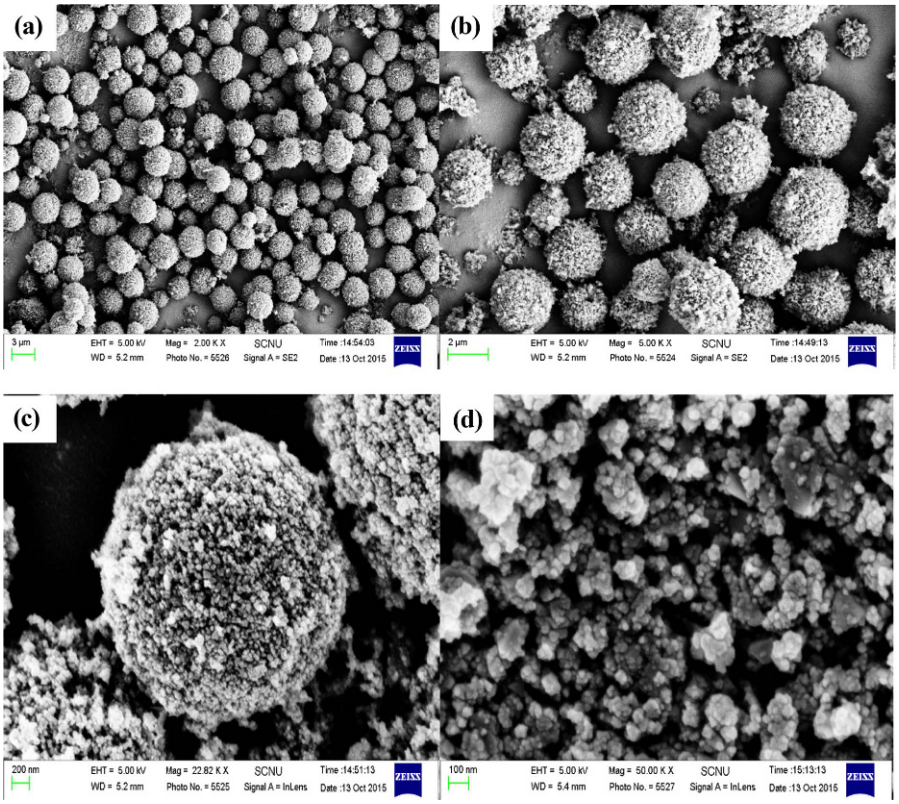

Fig. 2. (a), (b), (c), (d) SEM images with different magnifications; (e), (f) EDS spectrum; (g), (h), (i) elemental mapping of the $CoMn_2O_4$ microspheres.

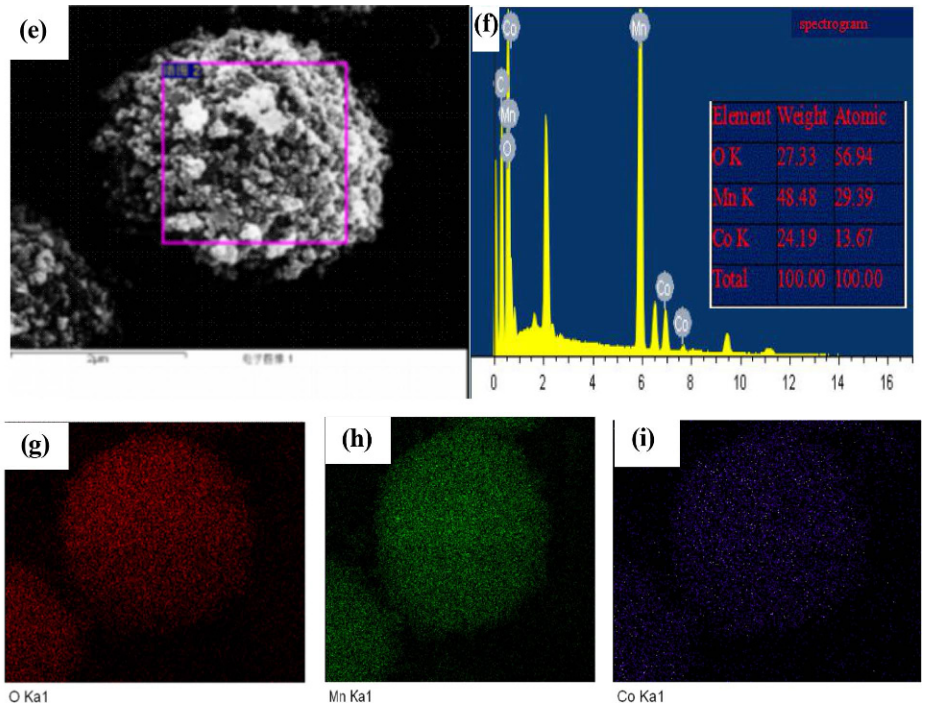

Fig. 2. Continued.

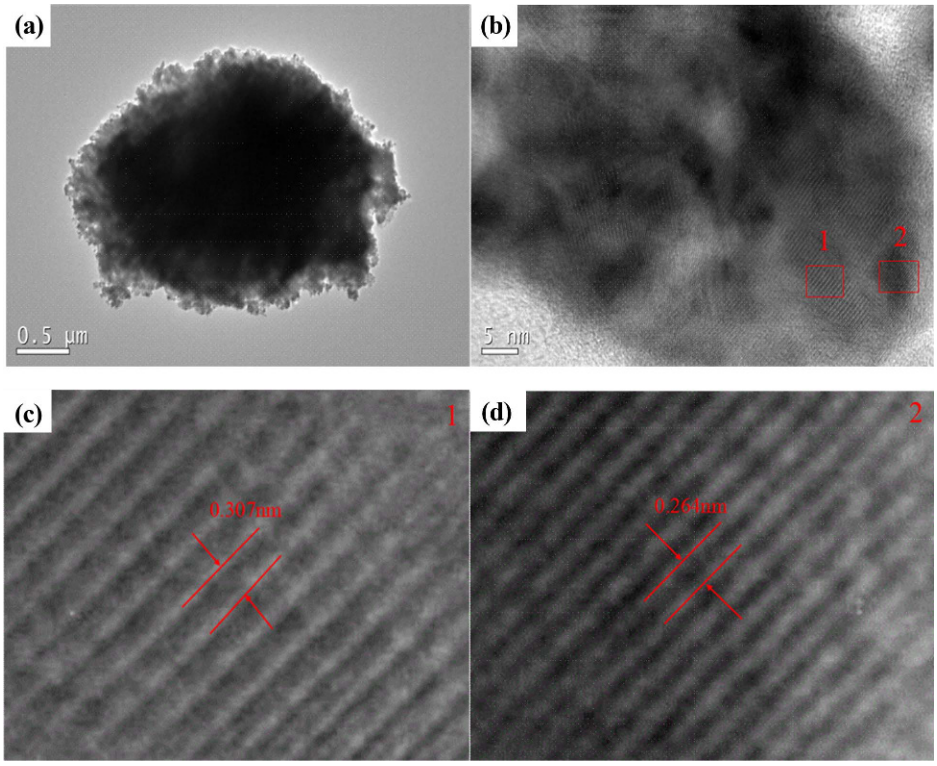

Fig. 3. (a), (b) TEM and HRTEM images of $CoMn_2O_4$ microspheres; (c), (d) High magnification TEM images of regions 1 and 2 in Fig. 2b.

microspheres are porous features constructed by stacking nanosized particles, which is consistent with the observation of the FESEM findings. High-resolution TEM images are shown in Fig. 3b. As observed in Fig. 3c, d, which are taken from the red square regions in Fig. 3b, clear lattice fringes with spacing of around 0.307 nm and 0.264 nm can be seen

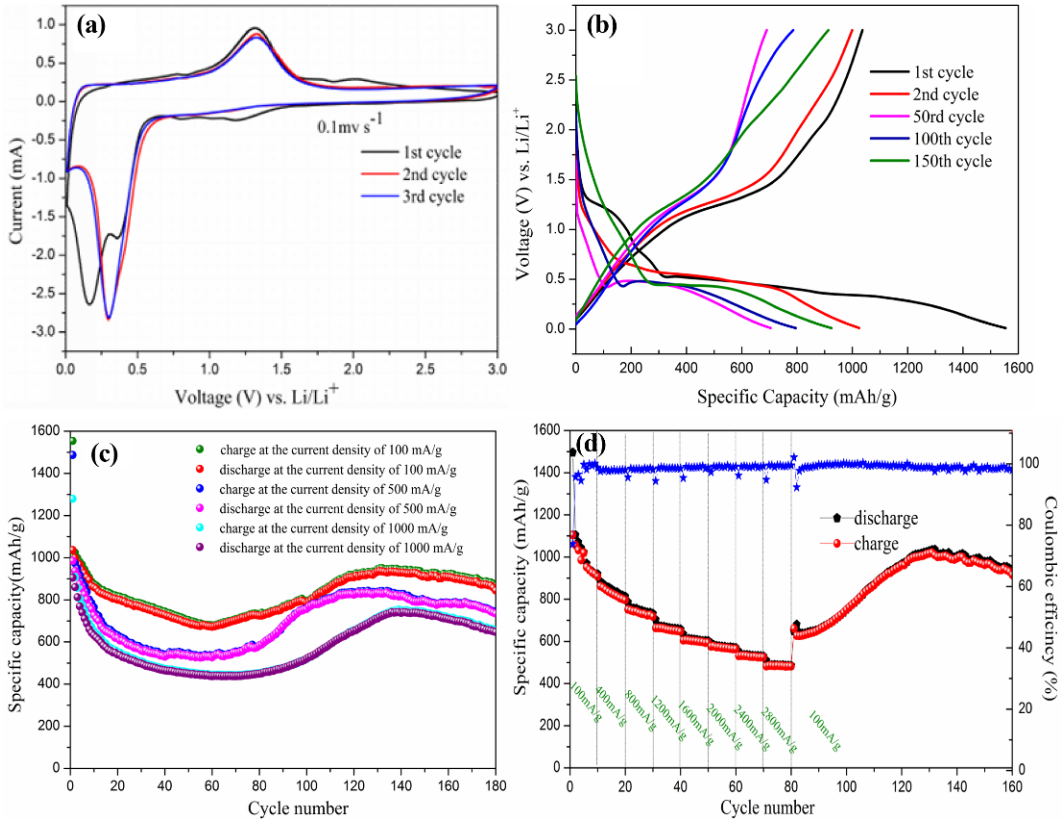

Fig. 4. Electrochemical properties of the $CoMn_2O_4$ microspheres electrodes: (a) cyclic voltammetry (CV) curves at a scan rate of 0.1 mV/s in the voltage window of 0.01-3.0 V, (b) discharge-charge voltage profiles, (c) charge-discharge capacities cycling performance recorded at a current density of 100 mA/g, 500 mA/g, 1000 mA/g, (d) charge-discharge capacities and coulombic efficiencies at different current densities.

obviously, corresponding to the inter-distance of the (112) and (103) crystal planes of the tetragonal $MnCo_2O_4$ phase, respectively. Thereby, it evidently revealed the single-crystal characteristics of the $CoMn_2O_4$ microspheres with good crystallinity.[21,22]

Here, the as-synthesized products are evaluated as anode materials for lithium-ion batteries. Figure 4a shows the cyclic voltammetry (CV) curves of porous $MnCo_2O_4$ microspheres electrode at a scan rate of 0.1 mV/s in the voltage range of 0.01-3.0 V versus Li/Li^+. In the first cathodic sweep, a broad peak centered at ~1.3 V could be ascribed to the reduction of Co^{3+} and Mn^{3+} to Co^{2+} and Mn^{2+}, respectively. The two intense peak at ~0.165 V and ~0.36 V could be assigned to the further reduction of Co^{2+} and Mn^{2+} to metallic Co and Mn, respectively. The intense oxidation peaks are observed at ~1.3 V in the anodic scan, corresponding to the oxidation of Mn to Mn^{2+} and Co to Co^{2+}.[23-25] The main reduction peaks shift in the subsequent cycles. From the second cycles, the reduction and oxidation peaks in the CV tests substantially overlapped, indicating a good reversibility of the redox reaction. Based on the CV curves, together with the storage mechanisms of $MnCo_2O_4$ that have been previously reported,[26,27] the entire electrochemical process can be expressed as follows:

$$MnCo_2O_4 + 8Li^+ + 8e \rightarrow Mn + 2Co + 4Li_2O \quad (1)$$

$$Mn + 2Co + 3Li_2O \rightarrow MnO + 2CoO + 6Li^+ + 6e \quad (2)$$

With a voltage window of 0.01-3.0 V, the plot of the specific capacity versus voltage (vs. Li/Li^+) at a current rate of 100 mA/g is illustrated in Fig. 4b. It is amazing that the as-synthesized $CoMn_2O_4$ microspheres deliver an extremely high initial discharge capacity and charge capacities of 1546 mAh/gand 1036 mAh/g, which is higher than the theoretical value 906 mAh/g based on equations (1). The extra capacity could be associated with the decomposition of the electrolyte at low voltages that generates a SEI film.[28] The decreasing specific capacity for $CoMn_2O_4$ electrodes may be ascribed to the reversible growth of a polymeric gel-like Film resulting from electrolyte degradation, which has also been observed in nanostructured $ZnMn_2O_4$.[29,30] The slope at about 1.25-0.5 V corresponds to the irreversible decomposition of electrolytes on the surface of $CoMn_2O_4$ microspheres, which results in the formation of a solid electrolyte interface (SEI) film on the electrode surface. It is confirmed by the fact that this plateau disappears in the subsequent cycles.[31,32]

Figure 4c depicts the cycling performance of the $CoMn_2O_4$ microspheres electrode at a current density of 100, 500, 1000 mA/g. During the first several cycles, there is a relatively high capacity loss. The discharge capacity is reduced to is 677, 525, 438 mA/g in the 60th cycle, which loses about 34.7%, 46.5%, 51.5% compared to the second cycle, respectively. This phenomenon is also observed in other transition metal oxide electrode materials, which is ascribed to the formation of a stable SEI layer on the electrode surface as well as the establishment of a compact electric contact with the current collector during the initial cycles.[33,34] Around the 70th cycle, the discharge capacities begin to increase. After the 180th cycle, the discharge specific capacity is able to return to 844, 734, 648 mA/g, respectively. This phenomenon may be ascribed to the formation of a polymeric surface film attached to the active or the reversible growth of a polymeric gel-like film resulting from kinetically activated electrolyte degradation.[35-37]

Figure 4d displays the cycling performance of $CoMn_2O_4$ microspheres at various current densities (100-2800 mA/g). The $CoMn_2O_4$ microspheres exhibit discharge capacities of 840, 745, 668, 613, 580, 536, 485 mAh/g at current densities of 400, 800, 1200, 1600, 2000, 2400 and 2800 mA/g, respectively. Moreover, the specific capacity is able to return to 1029 mAh/g when the current density is again reduced to 100 mA/g. It is obvious that the as-synthesized $CoMn_2O_4$ microspheres exhibit much improved cyclic capacity retention and rate capability. The improved electro-chemical performance of the as-prepared $CoMn_2O_4$ microspheres can be ascribed to their porous nanostructure, which can provide a larger surface area than the particles and bulk materials. The extra space can store more lithium ions, buffer the large volume change to some extent and decrease lithium ions diffusion length simulta-neously, leading to improvement in cycling capacity retention upon extended cycling.[38-40]

Whereas, as for the relatively low coulombic efficiency, We provided some suggestions: First, the surface area of as-synthesized material can be tuned using the annealing temperature. The large diameter and small surface area may be beneficial for improving the initical coulomb efficiency.[41] Second, Tan et.al reported that the porous Sn-C composite after a surface carbon encapsulation process through a chemical vapour deposition process showed a higher initial coulomb efficiency.[42] Third, Wang *et al.* prepared core-shell-structured Co_3O_4@Li_2MnO. The synergetic effect eliminates the huge irreversible capacity loss of Li_2MnO_3 during the initial charging process.[15] The similiar core-shell structured PPy@MoO_3 and PPy@V_2O_5 also showed huge reversible.[43,44]

4. CONCLUSIONS

In summary, We have developed a facile and green strategy to synthesize $CoMn_2O_4$ microspheres assembled by numerous closely packed primary nanoparticle in the size of 20-100 nm for lithium ion battery. The as-obtained $CoMn_2O_4$ microspheres delivers an initial discharge specific capacity of approximately 1546 mAh/g with a coulombic efficiency of 67.0% at a current rate of 100 mA/g and remarkable specific capacities (1029-485 mAh/g) at various current rates (100-2800 mA/g) and good cycling stability for highly reversible lithium storage. The exhibit excellent properties could be attributed to the unique mesoporous hierarchical micro/nanostructures and the possible synergetic effects of different metal ions. Moreover, it should be noted that the method could be extended to synthesize other metal oxides with novel hierarchical architectures.

ACKNOWLEDGEMENTS

The Scientific and Technological Plan of Guangdong Province (2016A0505030, 2016B010114002), the Natural Science Foundation of Guangdong Province (2014A030313436), The Scientific and Technological Plan of Guangzhou City (201607010322, 201607010274).

REFERENCES

1. L. X. Zhang, Y. L. Wang, H. F. Jiu, W. H. Zheng, J. X. Chang, and G. F. He, *Electrochim. Acta* **182**, 550 (2015).
2. N. H. Zhao, G. J. Wang, Y. Huang, B. Wang, B. D. Yao, and Y. P. Wu, *Chem. Mater.* **20**, 2612 (2008).
3. Y. S. Zhu, F. X. Wang, L. L. Liu, S. Y. Xiao, Z. Chang, and Y. P. Wu, *Energy Environ. Sci.* **6**, 618 (2013).
4. R. Marom, S. F. Amalraj, N. Leifer, D. Jacob, and D. Aurbach, *J. Mater. Chem.* **21**, 9938 (2011).
5. P. G. Bruce, B. Scrosati, and J. M. Tarascon, *Angew. Chem. Int. Ed.* **47**, 2930 (2008).
6. S. K. Ujjain, P. Ahuja, and R. K. Sharma, *J. Mater. Chem.* A. **3**, 9925 (2015).
7. X. W. Li, S. L. Xiong, J. F. Li, X. Liang, J. Z. Wang, J. Bai, and Y. T. Qian, *Chem. Eur. J.* **19**, 11310 (2013).
8. Y. R. Liu, B. C. Zhang, J. K. Feng, and S. L. Xiong, *RSC Adv.* **5**, 26863 (2015).
9. L. Zhou, D. Y. Zhao, and X. W. Lou, *Adv. Mater.* **24**, 745 (2012).
10. G. D. Li, L. Q. Xu, Y. J. Zhai, and Y. P. Hou, *J. Mater. Chem. A.* **3**, 14298 (2015).
11. M. H. Kim, Y. J. Hong, and Y. C. Kang, *RSC Adv.* **3**, 13110 (2013).
12. J. F. Ye, W. Liu, J. G. Cai, S. Chen, X. W. Zhao, and H. H. Zhou, *J. Am. Chem. Soc.* **133**, 933 (2011).
13. X. J. Hou, X. F. Wang, B. Liu, Q. F. Wang, T. Luo, D. Chen, and G. Z. Shen, *Nanoscale* **6**, 8858 (2014).
14. S. M. Oh, S. T. Myung, Y. S. Choi, K. H. Ohd, and Y. K. Sun, *J. Mater. Chem.* **21**, 19368 (2011).

15. F. X. Wang, Z. Chang, X. W. Wang, Y. F. Wang, B. W. Chen, Y. S. Zhu, and Y. P. Wu, *J. Mater. Chem. A* **3**, 4840 (2015).
16. Y. R. Liu, B. C. Zhang, J. K. Feng, and S. L. Xiong, *RSC Adv.* **5**, 26863 (2015).
17. W. H. Guo, X. X. Ma, X. L. Zhang, Y. Q. Zhang, D. L. Yu, and X. Q. He, *RSC Adv.* **6**, 96436 (2016).
18. L. Hu, H. Zhong, X. R. Zheng, Y. M. Huang, P. Zhang, and Q. W. Chen, *Sci. Rep.* **2**, 986 (2012).
19. P. Stefan, H. Holger, S. Marco, M. Stefan, M. Valeriu, K. P. Annie, I. Sylvio, S. Ulrich, K. Lorenz, D. Viola, H. Svenja, and B. Wolfgang, *RSC Adv.* **3**, 23001 (2013).
20. L. Wang, X. Zhao, Y. H. Lu, M. W. Xu, D.W. Zhang, and R. S. Ruoff, *J. Electrochem. Soc.* **158**, A1379 (2011).
21. H. J. Fan, M. Knez, R. Scholz, K. Nielsch, E. Pippel, D. Hesse, M. Zacharias, and U. Gosele, *Nat. Mater.* **5**, 627 (2006).
22. H. J. Fan, M. Knez, R. Scholz, K. Nielsch, E. Pippel, D. Hesse, U. Gosele, and M. Zacharias, *Nanotechnology* **17**, 5157 (2006).
23. J. Li, S. Xiong, X. Li, and Y. Qian, *Nanoscale* **5**, 2045 (2013).
24. L. Hu, H. Zhong, X. Zheng, Y. Huang, P. Zhang, and Q. Chen, *Sci. Rep.* **2**, 986 (2012).
25. M. H. Kim, Y. J. Hong, and Y. C. Kang, *RSC Adv.* **3**, 13110 (2013).
26. G. Li, L. Xu, Y. Zhai, and Y. Hou, *J. Mater. Chem. A* **3**, 14298 (2015).
27. J. Li, J. Wang, X. Liang, Z. Zhang, H. Liu, and Y. Qian, *ACS Appl. Mater. Inter.* **6**, 24 (2014).
28. J. Wang, Q. Zhang, X. Li, B. Zhang, L. Mai, and K. Zhang, *Nano Energy* **12**, 437 (2015).
29. C. Fu, G. Li, D. Luo, X. Huang, J. Zheng, and L. Li, *ACS Appl. Mater. Inter.* **6**, 2439 (2014).
30. S. W. Kim, H. W. Lee, P. Muralidharan, D. H. Seo, W. S. Yoon, D. K. Kim, and K. Kang, *Nano Res.* **4**, 505 (2011).
31. H. Lai, J. Li, Z. Chen, and Z. Huang, *ACS Appl. Mater. Inter.* **4**, 2325 (2012).
32. M. V. Reddy, G. V. S. Rao, and B. V. R. Chowdari, *Chem. Rev.* **113**, 5364 (2013).
33. Z. Bai, N. Fan, C. Sun, Z. Ju, C. Guo, J. Yang, and Y. Qian, *Nanoscale* **5**, 2442 (2013).
34. X. Xu, J. Liang, H. Zhou, D. Lv, F. Liang, Z. Yang, S. Ding, and D. Yu, *J. Mater. Chem.* **1**, 2995 (2013).
35. X. Wang, X. Li, X. Sun, F. Li, Q. Liu, Q. Wang, and D. He, *J. Mater. Chem.* **21**, 3571 (2011).
36. G. Zhou, D. W. Wang, F. Li, L. Zhang, N. Li, Z. S. Wu, L. Wen, G. Q. Lu, and H. M. Cheng, *Chem. Mater.* **22**, 5306 (2010).
37. S. Grugeon, S. Laruelle, L. Dupont, and J. M. Tarascon, *Solid State Sci.* **5**, 895 (2003).
38. W. Luo, X. Hu, Y. Sun, and Y. Huang, *J. Mater. Chem.* **22**, 8916 (2012).
39. L. Mao, K. Zhang, H. S. O. Chan, and J. Wu, *J. Mater. Chem.* **22**, 1845 (2012).
40. Y. Zhang, Y. Wang, Y. Xie, T. Cheng, W. Lai, H. Pang, and W. Huang, *Nanoscale* **6**, 14354 (2014).
41. N. Du, Y. F. Xu, H. Zhang, J. X. Yu, C. X. Zhai, and D. R. Yang, *Inorg. Chem.* **50**, 3320 (2011).
42. Z. Tan, Z. H. Sun, H. H. Wang, Q. Guo, and D. S. Su, *J. Mater. Chem. A* **1**, 9462 (2013).
43. Q. Qu, Y. Zhu, X. Gao, and Y. Wu, *Adv. Energy Mater.* **2**, 950 (2012).
44. W. Tang, L. Liu, Y. Zhu, H. Sun, Y. Wu, and K. Zhu, *Energ. Environ. Sci.* **5**, 6909 (2012).